PAPER

Synthesis and characterization of a pH/temperature-dual responsive hydrogel with promising biocompatibility features for stimuli-responsive 5-FU delivery†

Purushottam Suryavanshi,[a] Shriram Mahajan, [ID][b] Sanjay K. Banerjee, [ID][b] Kapileswar Seth [ID]*[c] and Subham Banerjee [ID]*[a]

The tunable properties of stimuli-responsive copolymers or hydrogels enable their application in different fields such as biomedical engineering, tissue engineering, or even drug release. Here we introduce a new PNIPAM-based triblock copolymer material comprising a controlled amount of a novel hydrophobic crosslinker 2,4′-diacryloyloxy benzophenone (DABP) and acrylic acid (AAc) to achieve lower critical solution temperature (LCST) between ambient and body temperatures. The dual stimuli-responsive p(NIPAM-*co*-DABP-*co*-AAc) triblock copolymer material and hydrogel were synthesized, and their temperature and pH-responsive behaviors were systematically investigated. The hydrogel exhibited excellent temperature and pH-responsive properties with an LCST of around 30 °C. Moreover, the synthesized copolymer has been demonstrated to be nontoxic both *in vitro* and *in vivo*. When the hydrogel was preloaded with the model drug 5-fluorouracil (5-FU), the designed hydrogel released the drug in a temperature and pH-controlled fashion. It was observed that the prepared hydrogel has the ability to entrap 5-FU, and the loading is more than 85%. In the case of temperature-controlled release, we observed almost complete release of 5-FU at lower temperatures and sustained release behavior at higher temperatures. In addition, the hydrogel matrix was able to retard the release of 5-FU in an acidic environment and selectively release 5-FU in a basic environment. By realizing how the hydrogel properties influence the release of drugs from preloaded hydrogels, it is possible to design new materials with myriad applications in the drug delivery field.

1. Introduction

Hydrogels are gaining wide attention in the field of biomedical and drug-delivery engineering due to their mechanical correspondence with the cellular matrix and biocompatibility.[1] Additionally, they are three-dimensional crosslinked polymeric networks that have the ability to swell in aqueous solution, but not to dissolve.[2,3] They are extensively investigated for a plethora of reasons, covering many research areas, such as drug delivery excipients,[4] bioprinting,[5] biomedicine,[6] and tissue engineering.[7] Furthermore, the hydrogels can be designed to have the desired physical/chemical characteristics, such as their mechanical strength and their potential to load and release drug molecules, which further expand their possible application in controlled drug delivery.[8] As a result, smart hydrogels have attracted a lot of attention because they show phase changes or abrupt volume changes with respect to external stimuli such as temperature, pH, and ionic strength,[9,10] and several approaches have been developed based on their tunability.[11,12] Apart from this, some properties of hydrogels could limit their practical applications, such as the high water content of hydrogels, which causes the instant release of entrapped drug molecules from the hydrogel matrix.

Amongst the smart hydrogels used in biomedical systems, poly(*N*-isopropylacrylamide) (PNIPAM) has earned some special attention. Its phase transitions from a hydrated to a dehydrated state at 32 °C, which is close to human body temperature, motivate many researchers to conduct extensive research on this material.[13] In addition, the ease of synthesis of PNIPAM-based hydrogels/microgels and a wide range of chemical modifications that can be easily incorporated into the structures have also attracted many researchers to conduct extensive research on such materials. Additionally, their transition temperature and their response to other stimuli such as pH, electro/

[a] Department of Pharmaceutics, National Institute of Pharmaceutical Education and Research (NIPER)-Guwahati, Changsari 781101, Assam, India. E-mail: subham@niperguwahati.in

[b] Department of Biotechnology, NIPER-Guwahati, Changsari 781101, Assam, India

[c] Department of Medicinal Chemistry, NIPER-Guwahati, Changsari 781101, Assam, India. E-mail: kapileswar@niperguwahati.in

† Electronic supplementary information (ESI) available. See DOI: https://doi.org/10.1039/d4tb00168k

magnetic field, and light can be modified by copolymerizing with different functional additives.[14,15] For instance, J. C. Breger et al. prepared a thermo-magnetically responsive PNIPAM based hydrogel by copolymerizing NIPAM, acrylic acid (AAc) and polypropylene fumarate with iron oxide particles and showed the potential use of such microgrippers as soft robotics for various applications.[16] Apart from this, copolymerization of PNIPAM with AAc or methacrylic acid makes it a pH responsive material, which is attributed to the protonation and deprotonation of AAc below and above the pK_a of 4.25.[8] In addition to AAc, many other monomers such as phenyl boronic acid and amines are also used to synthesize dual stimuli responsive hydrogels using PNIPAM as a copolymerizing agent.[17,18] Apart from this, the fine hydrophilic–hydrophobic balance during the synthesis of PNIPAM based hydrogels for various drug delivery applications is also considered as an important aspect of such formulations. The LCST of such hydrogels can be modified through incorporation of hydrophilic/hydrophobic crosslinkers within the polymer network.[19]

Typically, the hydrogel systems that exhibit a LCST between ambient and body temperatures are the most promising candidates for the biomedical applications. In this context, copolymerization of PNIPAM with a hydrophilic moiety tends to increase the LCST of the system and in contrast to this the hydrophobic moiety decreases the LCST of the system.[20,21] In this respect, the most commonly used crosslinker is N,N'-methylene bis acrylamide, which tends to shift the LCST to higher temperature.[22] Our group, among others, has synthesized a PNIPAM based hydrogel by copolymerizing with AAc and showed its potential application in controlled drug delivery in response to the temperature and pH. However, nearly all these studies are associated with N,N'-methylene bis acrylamide as a crosslinker, increasing the LCST of the system.

As we all know, smart hydrogels that exhibit mutual response to multiple stimuli, like pH and temperature, have advantages over the hydrogels sensitive to one stimulus. Thus,

the objective of this study was to design a triblock copolymer and hydrogel with a controlled hydrophilic and hydrophobic balance using 2,4'-diacryloyloxy benzophenone (DABP) as a novel hydrophobic crosslinker for the first time and AAc as a hydrophilic, pH-sensitive monomer. The addition of this novel crosslinker provides the benefit of possible tailoring of LCST near the body temperature. Furthermore, the cooperative effect of pH and temperature on the small molecule entrapment and release was systematically discussed in detail in the present work. Using these data, we are able to understand how the hydrogel's chemical and physical properties affect the release of small molecules (e.g., 5-fluorouracil (5-FU)) and suggest the possible mechanism of interaction between the model drug and hydrogel matrix in terms of modulating drug release. In addition, to the best of our knowledge, the synthesized triblock copolymer p(NIPAM-co-DABP-co-AAc) was evaluated for the in vivo biocompatibility study for the first time.

2. Materials and methods

2.1. Materials

N-Isopropylacrylamide (NIPAM) (purity 97%), acrylic acid (AAc) (purity 99%), 2,2'-azobis(2-methylpropionitrile) (AIBN), 1,4-dioxane, dichloroethane (DCE), pyridine, N,N-diisopropylethylamine (DIEA) were procured from Sigma-Aldrich Chemicals. 2,4'-Dihydroxybenzophenone (purity >98%) and acrylic anhydride (purity >95%) were procured from TCI, India. All other analytical and microbiological chemicals were procured from Merck India.

2.2. Synthesis of p(NIPAM-co-DABP-co-AAc)

(A) Step-wise approach

Step 1: Synthesis of 2,4'-diacryloyloxy benzophenone (DABP). To a magnetically stirred mixture of 2,4'-dihydroxybenzophenone (0.214 gm, 1 mmol, 1 equiv.), DIEA (0.258 gm, 2 mmol,

Purushottam Suryavanshi received his master's degree in Pharmaceutics from NIPER-Guwahati (Assam, India) in 2021. He is now a PhD research scholar at the Department of Pharmaceutics, NIPER-Guwahati. His research activities focus on the synthesis of new materials for various 3D and 4D printing technologies and further exploration of their potential applications in customized drug delivery systems.

Purushottam Suryavanshi

Dr Subham Banerjee is currently working as an Associate Professor in the Department of Pharmaceutics, NIPER-Guwahati, Assam, India. He received his doctoral degree from the Birla Institute of Technology (BIT), Mesra in collaboration with the Defence Research Laboratory (DRL), DRDO, Tezpur, Assam in the year 2015. He is also a visiting staff faculty of the University of Texas (UT) at Austin, USA. Dr Banerjee published many international articles in peer-reviewed journals and bagged prestigious awards/recognitions. Dr Banerjee's research area focuses on pharmaceutical additive manufacturing (AM)/3D and 4D printing, new materials for pharmaceutical AM, and cutting-edge translational pharmaceutical research.

Subham Banerjee

This journal is © The Royal Society of Chemistry 2024

J. Mater. Chem. B, 2024, **12**, 5098–5110 | 5099

2 equiv.), and pyridine (32.3 μL, 0.2, 20 mol%) in DCE (3 mL), acrylic anhydride (0.229 mL, 2 mmol, 2 equiv.) was added in a nitrogen environment while maintaining moisture free conditions. The obtained mixture was heated to 65 °C in an oil bath for 12 h. After completion of the reaction (12 h, TLC), the mixture was cooled to room temperature. Then 20% NaCl, 20% NaHCO₃, and 20% HCl were added to the resultant reaction mixture to remove any unreacted impurities. The mixture was extracted with ethyl acetate (5 mL × 2). The ethyl acetate layer was separated and dried over anhydrous Na₂SO₄, filtered off, and evaporated to dryness under vacuum. The obtained crude product was purified by column chromatography (60–120 mesh silica gel) using ethyl acetate/n-hexane (16 : 84 v/v) as an eluent to get the compound of interest (compound **3**) as a pale-yellow semisolid mass (85%). TLC (ethyl acetate: n-hexane, 16 : 84 v/v: $R_f \approx 0.7$; ^{1}H NMR, CDCl₃, 400 MHz) δ (ppm): 7.78–7.75 (m, 2H), 7.53–7.47 (m, 2H), 7.29 (dt, J = 7.5, 1.1 Hz, 1H), 7.21–7.18 (m, 1H), 7.15 (d, J = 4.6 Hz, 1H), 7.13 (d, J = 2.0 Hz, 1H), 6.56 (dd, J = 17.3, 1.2 Hz, 1H), 6.29–6.26 (m, 1H), 6.25–6.22 (m, 1H), 5.99 (dd, J = 10.4, 1.4 Hz, 2H), 5.78 (dd, J = 10.5, 1.2 Hz, 1H); ^{13}C NMR (101 MHz, CDCl₃) δ (ppm): 195.57, 164.02, 153.84, 137.49, 135.12, 133.36, 132.52, 131.71, 129.98, 129.82, 128.37, 127.58, 121.53, 77.41, 77.38, 77.09, 77.08, 77.06, 76.77, 76.76, 76.74, 29.72; FT-IR ν_{max} (cm^{-1}): 3472.6, 3071.4, 2930.0, 2034.3, 1949.4, 1751.4, 1666.5, 1600.3, 1487.7, 1441.9, 1143.1; MS (ESI) (M + H)$^+$ = 322.87.

Step 2: Synthesis of p(NIPAM-co-DABP). The general synthetic procedure for the synthesis of p(NIPAM-co-DABP) is adapted from similar literature with slight modifications.[23,24] Briefly, DABP (0.028 g, 0.089 mmol, 1 equiv.) was dissolved in 1,4-dioxane with stirring at room temperature. To a magnetically stirred solution of DABP, NIPAM (1 g, 8.85 mmol, approximately 100 equiv.) was dissolved. The entire solution was degassed using N₂ for 30 min. After degassing, AIBN (0.01701 mL, 0.089 mmol, 1 equiv.) was added to the degassed reaction mixture, and the reaction vessel was tightly sealed and again degassed for 30 min prior to initiating the polymerization reaction. The degassed reaction vessel was heated at 70 °C in an oil bath and kept stirred at 100 rpm under a N₂ atmosphere for 12 h. The reaction mixture was cooled to room temperature and then 100 mL of diethyl ether was added to quench the polymerization process. The white-colored precipitate was filtered and dried using a vacuum oven at 40 °C. ^{1}H NMR, CD₃OD, 400 MHz δ (ppm): 7.64 (assigned to the N–H shift), 5.60–6.20 (assigned to the *para*-proton shift of the DABP moiety), 3.96 (assigned to the C–H shift of the NIPAM moiety), 1.14–3.65 (assigned to the C–H and CH₂ proton shifts of the p(NIPAM-co-DABP) chain; FT-IR ν_{max} (cm^{-1}): 3301.7 (N–H stretching), 2965.6 (CH=CH₂ stretching), 1754.2, 1642.2 (C=O stretching), 1525.6 (aromatic C=C stretching). The detailed strategy to confirm regio-selective copolymerization of PNIPAM with the *para*-acryloyl unit of DABP is given in the ESI.†

Step 3: Synthesis of p(NIPAM-co-DABP-co-AAc). p(NIPAM-co-DABP) (1 g) was dissolved in 1,4-dioxane with stirring at room temperature. The resultant solution was kept aside with stirring until a clear solution was formed. To the clear solution, acrylic acid (0.108 g, 1.60 mmol) was added, and the resultant reaction solution was sealed and degassed using N₂ gas for 30 minutes. The mole equivalent ratio of p(NIPAM-co-DABP) to acrylic acid was 1 : 10 equiv. To the degassed solution, AIBN (0.01701 mL, 0.089 mmol) was added, and the sealed reaction vessel was degassed again for 30 minutes. The degassed reaction vessel was heated at 70 °C in an oil bath and kept stirred at 100 rpm under a N₂ atmosphere for 12 h. The reaction mixture was cooled to room temperature and then 100 mL of diethyl ether was added to quench the polymerization process. The white-colored product was filtered and dried using a vacuum oven at 40 °C. ^{1}H NMR, DMSO, 400 MHz) δ (ppm): 12.03 (assigned to the O–H shift), 7.94 (assigned to the N–H shift), 7.17–7.19 (aromatic proton shift), 5.53–6.22 (assigned to the *para*-proton shift of the DABP moiety), 1.04–3.93 (assigned to the C–H and CH₂ proton shifts of the p(NIPAM-co-DABP-co-AAc) chain.

(B) One-pot multicomponent synthesis of p(NIPAM-co-DABP-co-AAc). The one-pot multicomponent synthesis of p(NIPAM-co-DABP-co-AAc) was performed as follows: the general synthetic scheme was adapted from a similar literature with a slight change in the molar ratio of monomers and the crosslinker.[25] To a magnetically stirred solution of DABP (0.028 g, 0.089 mmol, 1 equiv.) in 1,4-dioxane, NIPAM (1 g, 8.85 mmol, approximately 100 equiv.) and acrylic acid (0.108 g, 1.60 mmol, approximately 18 equiv.) were added with constant stirring at room temperature. The reaction vessel was sealed properly, and the reaction solution was purged with N₂ gas for 30 minutes. After degassing, AIBN (160 μL, 1.08 mmol) was added with stirring. The resultant mixture was degassed using N₂ gas for 30 minutes. The degassed reaction vessel was placed in an oil bath, which was previously maintained at 70 °C and kept overnight at 100 rpm in an N₂ environment for 12 h. The reaction mixture was cooled to room temperature and then 100 mL of diethyl ether was added to quench the polymerization process. The white-colored product was filtered and dried using a vacuum oven at 40 °C. ^{1}H NMR, DMSO, 400 MHz δ (ppm): 12.02 (assigned to the O–H shift), 7.93 (assigned to the N–H shift), 7.15–7.20 (assigned to the aromatic proton shift), 5.53–6.60 (assigned to the *para*-proton shift of the DABP moiety), 1.05–3.84 (assigned to the C–H and CH₂ proton shifts of the p(NIPAM-co-DABP-co-AAc) chain. It is noted that from here onwards, all other characterizations were performed on p(NIPAM-co-DABP-co-AAc) synthesized by a one pot synthesis method.

2.3. Characterization of p(NIPAM-co-DABP-co-AAc)

2.3.1. Chemical characterization

FT-IR spectroscopy. FT-IR spectroscopy was performed in the ATR mode (Alpha 2, Bruker, Germany) in a scanning range of 600–4000 cm^{-1}. The obtained data were plotted as %transmittance *vs.* wavenumber (cm^{-1}).

X-ray photoelectron spectroscopy (XPS). The elemental composition was analyzed using XPS measurements. The

5100 | *J. Mater. Chem. B*, 2024, **12**, 5098–5110

This journal is © The Royal Society of Chemistry 2024

experiments were performed using the PHI Versa probe III system (physical electronics – USA) equipped with an Al-Kα source. The source was set to illuminate a spot size of 200 microns. While experimenting, the electron gun was used to prevent sample charging. Furthermore, the wide-scan XPS spectrum was collected and deconvoluted using the origin lab software for further analysis.

2.3.2. Thermal and crystalline properties assessment

Differential scanning calorimetry (DSC). DSC analysis was performed using a DSC thermal analysis instrument (DSC-3, STARe System, Mettler Toledo, Switzerland). All the samples were accurately weighed (4–5 mg) and placed in an aluminum crucible. The DSC analysis was performed from 0 to 150 °C in an N_2 environment at 10 °C min^{-1}.

Thermogravimetric analysis (TGA). The weight loss of the synthesized compound with respect to the temperature was analyzed using TGA (TGA-2 STARe system, Mettler Toledo, Switzerland). Furthermore, the obtained results were used to determine the compositional properties of the compound. The accurately weighed samples were transferred to an aluminum oxide crucible. The TG analysis was performed from ambient temperature to 900 °C in an N_2 gas environment.

X-ray diffraction analysis. XRD analysis was performed using an XRD diffractometer (EMPYREAN XRD, Malvern Panalytical, United Kingdom). The diffractogram was recorded with a K-α wavelength of 1.5406 Å with Cu as an anode at 40 kV and 40 mA in the 2θ range of 5–80°.

2.3.3. Matrix-assisted laser desorption ionization–time-of-flight (MALDI-ToF) mass spectrometry.

The MALDI-ToF/MS spectra of the synthesized compound were recorded using a Bruker Autoflex Speed MALDI-ToF/MS spectrometer with a molecular mass range of 1000–10 000 Da in the linear mode using sinapinic acid as a matrix (2 mg mL^{-1} in THF). The nitrogen laser, which has a wavelength of 337 nm and a pulse frequency of 200 MHz, was used to accelerate the ions. The synthesized compound was dissolved in THF (1 mg mL^{-1}) until a clear solution was formed. The matrix (20 μL) and the polymer solution (20 μL) were mixed together and dried on the steel target plate to acquire MALDI-ToF/MS spectra.

2.4. Temperature/pH-responsive p(NIPAM-*co*-DABP-*co*-AAc)

Dynamic light scattering (DLS) measurement. The hydrodynamic diameter as a function of pH and temperature was assessed using the DLS technique.[25] The synthesized compound was suspended in the aqueous solution with different pH values, such as 1.2, 3.0, 6.8, and 7.4. The prepared aqueous suspension was filtered using a 0.45-micron syringe filter, and the filtrate was analyzed using a particle size analyzer (Nano-ZS, Malvern Instruments Ltd). For temperature-dependent studies, the SOP was created in the 20–50 °C temperature range with an increment of 2 °C. At each temperature, the particle size measurement was performed and a plot of particle size *vs.* temperature was constructed, which was further used to determine the lower critical solution temperature (LCST) of the p(NIPAM-*co*-DABP-*co*-AAc) polymer system.

Variable temperature NMR spectroscopy. The variable temperature ^{1}H NMR spectra at room temperature and 50 °C were recorded using D_2O as a solvent system and a Bruker AVANCE Neo 400 MHz spectrometer to observe the temperature-dependent behavior of the molecule.

FT-IR spectroscopy. The pH-responsive FT-IR analysis was performed in the ATR mode (Alpha 2, Bruker, Germany). The 20 mg mL^{-1} polymer solution was prepared using different pH solutions (pH 1.2, 3.0, 6.8, and 7.4) and kept aside for 5 minutes at room temperature. The FT-IR spectra were recorded for each sample in the scanning range of 800–2400 cm^{-1}. The obtained data were plotted as % transmittance *vs.* wavenumber (cm^{-1}) for further analysis.

UV-visible spectroscopy. pH-dependent UV-visible absorbance of the synthesized compound was determined using a UV-visible spectrophotometer (Shimadzu 1900, Japan). The synthesized polymer was dissolved in the aqueous solution with different pH values (1.2, 3.0, 6.8, and 7.4); whenever necessary, a probe sonicator was used. The prepared polymer solution was filtered using a 0.45-micron syringe filter and analyzed using a UV-visible spectrophotometer in a 200–800 nm wavelength range.

2.5. Cytotoxicity assessment

The cytotoxicity of the polymer was estimated by MTT viability assay. The fine powder of the polymer was dispersed in phosphate-buffered saline (PBS). HEK-293 and HT-29 cells were seeded in 96 well plates at 12 000 cells per well in 200 μL of the medium. After reaching a cell confluency of up to 80%, the suspension of polymer powder was added to the wells at different concentrations (0 to 1000 μg mL^{-1}). Then the cells were further incubated for another 24 h, and after that, 50 μL of MTT solution (0.4 mg mL^{-1}) in PBS were added to each well and incubated at 37 °C in 5% CO_2 for 4 h. Then, after removing the MTT solution carefully, the formed formazan crystals were solubilized in dimethyl sulfoxide (DMSO). The absorbance was measured using a Spectramax iD3 instrument (Molecular Devices, LLC, San Jose, CA) at 492 nm. PBS-treated cells with 100% viability were used as controls.

2.6. Acute oral toxicity study

2.6.1. General considerations.

The acute oral toxicity assessment of the synthesized compound was conducted as per the OECD 423 guidelines.[26] A total of 12 Sprague-Dawley (SD) rats aged between 6 and 7 weeks were taken from the Central Animal House Facility (CAF), NIPER-G, Assam, India (IAEC approval no.: NIPER/PE/2023/19). All the animals were familiarized to the working environment for 1 week prior to the initiation of the study. All tests and procedures were conducted in compliance with the Institutional Animal Ethics Committee (IAEC) formed under the supervision of CPCSEA under the Ministry of Animal Welfare Division of the Government of India, New Delhi.

2.6.2. Methodology.

All animals were categorized into two groups, namely the control group and test group, with each group containing 6 animals. The synthesized triblock

This journal is © The Royal Society of Chemistry 2024

J. Mater. Chem. B, 2024, **12**, 5098–5110 | **5101**

copyright p(NIPAM-*co*-DABP-*co*-AAc), at a dose of 2000 mg kg^{-1}, was administered to the test group using PBS solution as a vehicle. The remaining 6 animals received the same volume of vehicle (PBS solution) that was considered as a control group. All the experimental animals were cautiously observed for any behavioral changes and mortality, immediately after the dosing, at 2 and 4 h intervals and subsequently at days 1, 7, and 14. The blood samples were collected on respective days for further haematological and serum biochemical analyses. At the end of the study, *i.e.*, on day 14, the animals were humanly sacrificed, and an autopsy was carried out to collect the major organs for any organ level toxicity observations.

2.6.2.1. Hematological and biochemical analyses. The blood samples (approximately 0.2 mL) were collected from the retro-orbital plexus of each rat at days 0, 1, 7, and 14 and kept in earlier coated K2-EDTA vials (BD Microtainer® vial). The collected unprocessed blood samples were used to determine various haematological parameters such as haemoglobin, total RBC, WBC, platelets, *etc.* using a differential haematology analyser (Celltac alpha, Nihon Kohden India Pvt. Ltd, India). The serum samples (approximately 200 μL) were collected at predetermined day intervals and stored at −80 °C prior to the serum biochemical analysis. The biochemical parameters, including the liver function test (aspartate aminotransferase, AST; alanine aminotransferase, ALT) and kidney function test (creatinine), were determined using a serum biochemistry analyzer (RX Daytona+, Randox Laboratories Ltd, UK). Statistical analysis was performed using graph pad prism 8.0.

2.6.2.2. Histopathology. All animals were sacrificed on day 14, and the autopsy was carried out to collect the major organs such as the liver, kidney, and intestine, the organs which are involved in the metabolism, absorption, and excretion processes of molecules. The collected organs were stored in 10% formalin solution followed by dehydration with ethanol for 1 h. The fully dehydrated tissue sample was treated with acetone and xylene and fixed in a paraffin wax. The slices of 4 μm thickness were obtained using a microtome and the prepared slices were subjected to haematoxylin and eosin staining. After treating with haematoxylin and eosin the sections were washed with ethanol, acetone, and xylene for 5 min each and mounted using DPX. The dried sections were visualized using high-power digital optical microscopy. The optical images of the tissue samples were taken at 10× and 20× magnifications.

2.7. Model drug loading

5-Flurouracil (5-FU) as a model drug was loaded into the synthesized hydrogels using a swelling-diffusion method.[27] The 5-FU solution of 1 mg mL^{-1} concentration was prepared in phosphate buffer (pH 7.4). After the formation of a clear solution, the dried hydrogel sample was accurately weighed between 100 and 110 mg and carefully mixed with the drug solution and kept aside for swelling for 24 h at 37 °C for the temperature-dependent and pH-dependent release study. After the swelling equilibrium was achieved, the swelled hydrogels

were washed with 0.1 N HCl solution maintained at 37 °C. The washing procedure was performed three times to remove the free drug. The 5-FU loaded hydrogels were collected using a centrifugation method, and the supernatant was collected to determine the free drug using a UV-visible spectrophotometer (UV2600, Shimadzu, Japan) at a wavelength of 263 nm.

2.8. *In vitro* release study

To observe the dual-stimuli responsive release of 5-FU from the hydrogel, the 5-FU loaded hydrogel samples were transferred to a dialysis bag (MWCO = 14 000 Da), and for the temperature-controlled release experiment, the study was conducted at two different temperatures based on the LCST of the synthesized material in the aqueous medium. Briefly, the 5-FU loaded hydrogel samples were transferred to a beaker filled with 80 mL of double distilled water, which was maintained below LCST (24 °C) and above LCST (40 °C). The solution was stirred continuously at 100 rpm throughout the study. At predetermined time intervals (0–24 h), an aliquot of 1 mL was collected and analysed for % cumulative drug release (% CDR) using a UV-visible spectrophotometer (UV2600, Shimadzu, Japan) at a wavelength of 263 nm. Similarly, to study the pH-controlled release of 5-FU, the experiment was conducted at two different pH values based on the pK_a of acrylic acid (pK_a = 4.25). For this experiment, the 5-FU loaded hydrogel samples were transferred to a beaker filled with 80 mL of an aqueous solution having a pH of 1.2 at 37 °C at 100 rpm. At predetermined time intervals (0–4 h) 1 mL of aliquot was collected and analysed for % CDR. After 4 h, the pH of the solution was increased to 6.8 using 0.01 M phosphate buffer; at selected time intervals 1 mL of the sample was collected from each beaker and analysed for % CDR using a UV-visible spectrophotometer. It is noted that the all-release experiments were carried out in triplicate to avoid any statistical error and the data were represented as mean ± SD.

3. Results and discussion

3.1. Chemical characterization of p(NIPAM-*co*-DABP-*co*-AAc)

The FT-IR spectra of p(NIPAM-*co*-DABP-*co*-AAc) are shown in Fig. 1. The observed band at 3270.66 cm^{-1} confirms the presence of amine (N–H) stretching in the polymer network, which supports the presence of the crosslinked NIPAM moiety. Apart from this band, we observed a stretching band at 3068.66 cm^{-1} and 2969.64 cm^{-1}, which confirms the presence of the carboxylic group and CH$_3$ stretching in the structure, indicating successful copolymerization of AAc and NIPAM within the co-polymer network. In addition, the characteristics peaks at 1718.62 (ester C=O), l628.65 (amide C=O), and 1526.67 (ketone C=O)[28] confirm the C=O group derived from AAc, NIPAM, and DABP respectively. In addition, the peak at 1449.29 cm^{-1} proves the presence of the C–O group. Overall, the obtained results confirm the copolymerization of NIPAM and AAc with DABP.

In addition to the FT-IR study, the exhaustive compositional analysis of the p(NIPAM-*co*-DABP-*co*-AAc) triblock copolymer
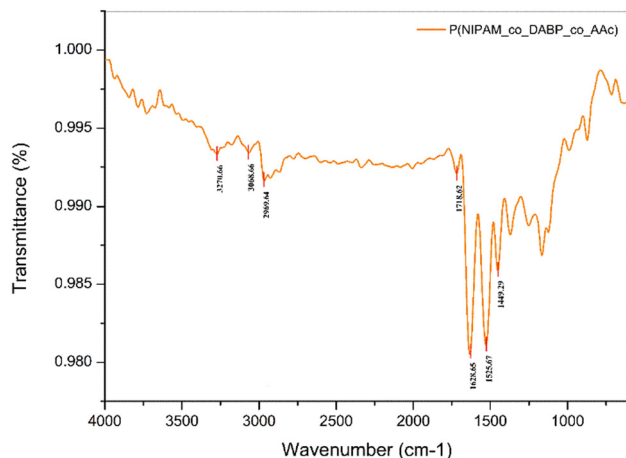
5102 | *J. Mater. Chem. B*, 2024, **12**, 5098–5110

This journal is © The Royal Society of Chemistry 2024

Fig. 1 FT-IR spectra of p(NIPAM-*co*-DABP-*co*-AAc).

was performed using a non-destructive spectroscopy technique known as X-ray photoelectron spectroscopy (XPS). Fig. 2a shows a wide XPS spectrum of p(NIPAM-*co*-DABP-*co*-AAc), which includes carbon (C 1s) spectra at 282–290 eV, nitrogen spectra at 396–404 eV, and oxygen (O 1s) spectra at 528–536 eV, attesting successful copolymerization of NIPAM, DABP, and AAc.

The peaks at around 284.5 eV, 284.8 eV, and 288.0 eV were observed in the high-resolution C 1s spectrum (Fig. 2b), indicating the presence of C=C, C–C/C–H, and C=O groups in the copolymer structure. In addition, the peaks at around 398 eV and 399 eV in the N 1s spectrum (Fig. 2c) are attributed to the C–N and N–H groups respectively. The presence of these groups indicates the incorporation of the NIPAM monomer in the p(NIPAM-*co*-DABP-*co*-AAc) system. Furthermore, we observed two peaks at around 531 and 532 eV in the O 1s spectra, which correspond to the C=O and O–H groups of AAc and DABP respectively, which were copolymerized in the p(NIPAM-*co*-DABP-*co*-AAc) system. To boot, the obtained findings are compared with the available literature.[29] Hence, the obtained XPS findings confirmed the copolymerization of NIPAM, DABP, and AAc monomers in the p(NIPAM-*co*-DABP-*co*-AAc) system.

3.2. Thermal and crystalline properties of p(NIPAM-*co*-DABP-*co*-AAc)

Fig. 3 shows the DSC findings of the triblock copolymer p(NIPAM-*co*-DABP-*co*-AAc). The copolymer showed large endothermic transition in the studied region. The onset of the endotherm is considered as the transition temperature of the thermo responsive triblock copolymer when exposed to heating, where bonded water molecules are removed from the polymer network and the system undergoes intramolecular coil-to-globule transition, assembling polymer chains resulting in polymer precipitation. From the obtained data, the transition temperature of the synthesized copolymer system was found to be around 30.89 °C, where the phase transition of the copolymer system took place. The NIPAM based polymer has a fixed phase transition temperature, *i.e.*, LCST at around 32 °C, and it is possible to tune the LCST of this system by grafting it with hydrophobic and hydrophilic moieties.[30]

Usually, the biomedical applications demand the LCST of the polymer system to be between 32 and 37 °C or rapid swelling–deswelling behaviour in response to the temperature or any other stimuli such as pH. In relation to this, S. J. Lue *et al.* modified the LCST of PNIPAM by incorporating AAc as a hydrophilic monomer. The authors showed that with an increase in the concentration of AAc, there is an increase of the LCST of the PNIPAM-based hydrogel system from 34.82 to 43.96 °C.[21] On the other hand, the incorporation of a hydrophobic moiety leads to a decrease in the LCST of the system. S. Tang *et al.* prepared the PNIPAM hydrogels by incorporating hydrophobic 4,4′-dihydroxy biphenyl diacrylate as a crosslinker and reported a decrease in LCST with an increasing amount of crosslinker from 32.8 °C to 4.3 °C.[30] In our findings the LCST of the synthesized triblock copolymer system shifted to 30.89 °C from 32 °C, which was envisioned as a controlled hydrophobic–hydrophilic balance during grafting of the PNIPAM moiety with DABP and AAc respectively. The obtained LCST findings could enable the potential use of such triblock copolymers with a controlled hydrophilic–hydrophobic balance in various biomedical applications. Furthermore, the single glass transition temperature (T_g) was obtained for the synthesized triblock copolymer at around 66.65 °C; indeed, such triblock copolymer systems generally display multiple T_g behaviour. Hence, based on the findings we can confirm that the synthesized system possess a good miscibility between the copolymers with strong intermolecular hydrogen bonding.[31]

The detailed thermal degradation and compositional analysis of the p(NIPAM-*co*-DABP-*co*-AAc) triblock copolymer in comparison to the raw materials was performed using TGA. The obtained data are shown in Fig. 4. The TGA analysis was performed in the 25 °C to 500 °C range. In the case of AAc and NIPAM, we observed maximum thermal degradation in the range of 100 to 200 °C. Furthermore, to determine the precise degradation temperature at which maximum weight loss occurred, we plotted the first derivative graph as shown in Fig. S11 (ESI†). From the first derivative graph, the maximum weight loss was observed at 138.82 °C and 165.25 °C for AAc and NIPAM, respectively (Fig. S11A and B, ESI†). Furthermore, in the case of DABP we observed maximum weight loss in the temperature range of 350–450 °C, with a maximum weight loss at 402.69 °C (Fig. S11C, ESI†). In the case of p(NIPAM-*co*-DABP-*co*-AAc) two thermal events were observed: firstly, in the range of 50–150 °C and secondly, in the range of 300–450 °C. The first derivative of the same is shown in Fig. S11D (ESI†), which reveals that the initial degradation at 56.14 °C is due to the water loss with maximum weight loss at 413.91 °C. This may be due to the degradation of the side chain functional group and backbone structure. Overall, the obtained findings confirm the two important leads: first, the incorporation of AAc and DABP in the PNIPAM chain had a significant impact on the thermal stability of the system and second, it confirms incorporation of AAc and DABP within the p(NIPAM-*co*-DABP-*co*-AAc) copolymer network.

Furthermore, the crystalline properties of the p(NIPAM-*co*-DABP-*co*-AAc) triblock copolymer were investigated using XRD analysis. Fig. 5 shows the XRD findings of the p(NIPAM-*co*-
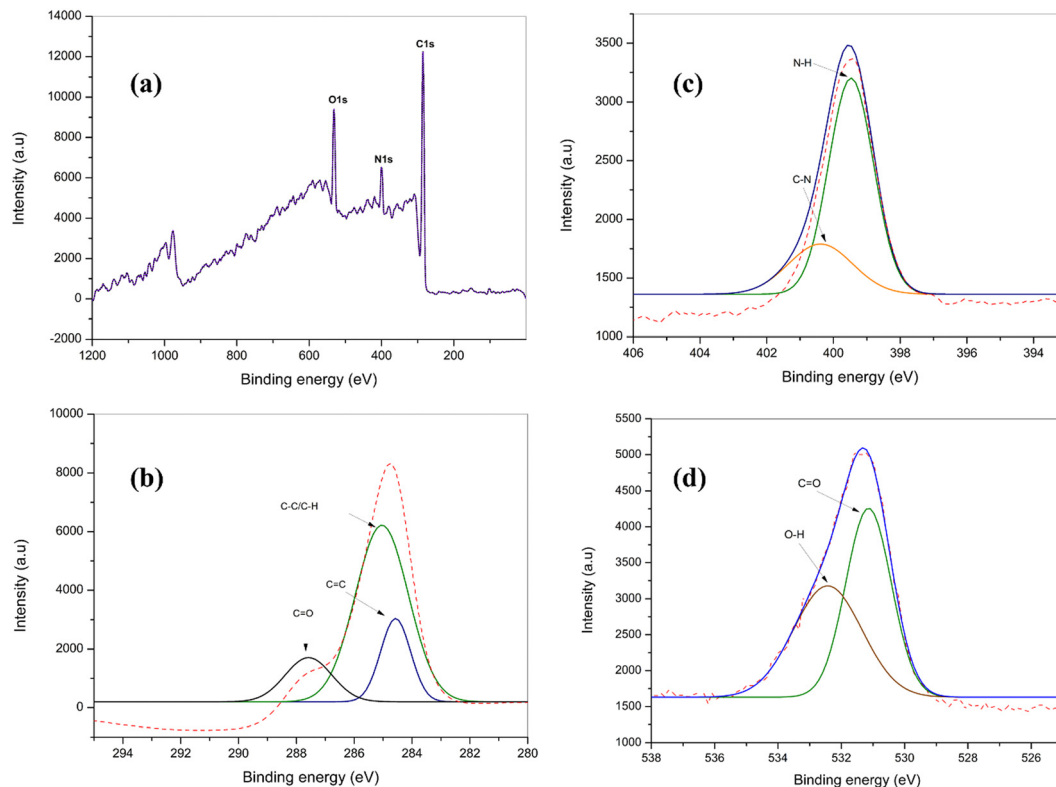
Fig. 2 XPS spectrum of the triblock copolymer p(NIPAM-*co*-DABP-*co*-AAc): (a) wide XPS spectrum, (b) high-resolution C 1s XPS spectrum, (c) high-resolution N 1s XPS spectrum, and (d) high-resolution O 1s XPS spectrum.
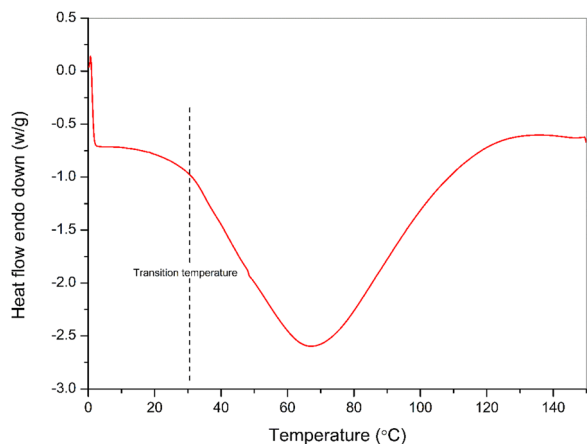

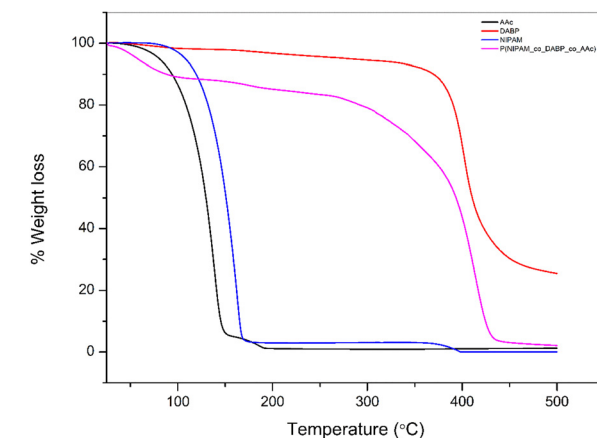**Fig. 3** DSC thermogram of the p(NIPAM-*co*-DABP-*co*-AAc) triblock copolymer.

Fig. 4 TGA thermograms of AAc, NIPAM, DABP and p(NIPAM-*co*-DABP-*co*-AAc).

DABP-*co*-AAc) triblock copolymer: the broad native peaks at 8.98°, 20.75°, and 39.6° suggest the amorphous phase of the synthesized triblock copolymer. Furthermore, the peaks at 8.98° and 20.75° are attributed to the interplanar distance between the associated polymer chains of PNIPAM, d_1 and d_2-spacings[32] respectively.

3.3. MALDI-ToF mass spectrometry analysis

MALDI-ToF analysis demonstrates its potential in the characterization of the polymeric system. Particularly, the technique is used to analyze the molecular weight and distribution of narrow polydispersity index polymers with high-resolution and accuracy.[33] The full MALDI-ToF spectrum of the triblock copolymer p(NIPAm-*co*-DABP-*co*-AAc) is shown in Fig. S12 (ESI†). The obtained mass spectrum contains several series of signals originating from the frequent statistically scattered monomers produced by the random copolymerization. The spectrum was deconvoluted in the 1000–1600 *m/z* region (Fig. 6), and the dominant peak series was obtained, such as peak series A at
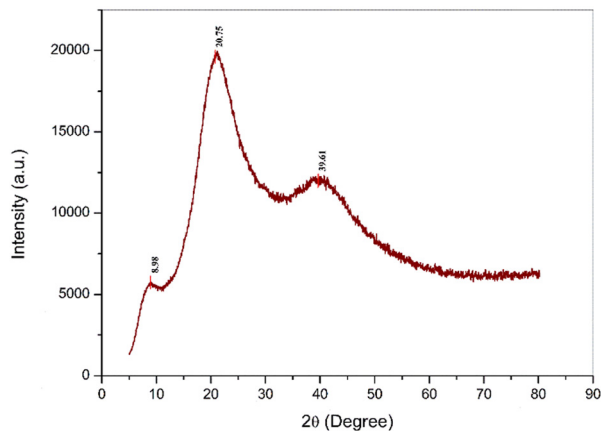
5104 | *J. Mater. Chem. B*, 2024, **12**, 5098–5110

This journal is © The Royal Society of Chemistry 2024

Fig. 5 XRD diffractogram of the p(NIPAM-*co*-DABP-*co*-AAc) triblock copolymer.

1018, 1131, 1244, 1358, and 1469 *m/z*, corresponding to $(113.16)_n$. In this context, *n* is the number of NIPAM units. The second major peak series, *i.e.*, peak series B, which corresponds to *m/z* at 1081, 1153, 1225, and 1440, was obtained, related to $(72.06)_m$, where *m* is the number of AAc units. Finally, the third peak series, named series C, was obtained at an *m/z* of 1289 related to 322×4, where 4 is the number of 2,4-di-ABP units. The obtained results confirmed that the copolymer was formed mainly by the chain transfer reaction. At the same time, spectra convey that the monomers are randomly copolymerized. The molecular weight range of the prepared triblock copolymer was found to be in the range of 1018–6440 *m/z*.

3.4. Temperature/pH-responsive properties of p(NIPAM-*co*-DABP-*co*-AAc)

Thermosensitive macromolecules can undergo a reversible coil–globule transition at certain temperatures, such as the LCST or upper critical solution temperature (UCST). A reversible coil-to-globule phase transition when immersed in an aqueous solution at its LCST is considered as an essential physiological property of PNIPAM. It demonstrates excellent the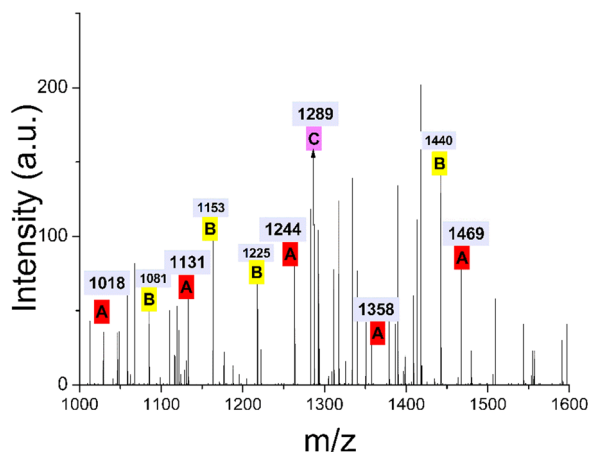rmoresponsive behavior both from a fundamental viewpoint and from a practical perspective. In response to the temperature change, the thermo-responsive polymer pNIPAM undergoes hydrophilic–hydrophobic transitions. Dynamic light scattering (DLS) can be used to assess such thermal transitions. A copolymer of this type also displays a unique phase transition at LCST from a swollen hydrated state to a shrunken dehydrated state. From the DLS measurement, we can see that synthesized p(NIPAM-*co*-DABP-*co*-AAc) shows a unique temperature-sensitive behavior, as shown in Fig. 7, indicating a change in the particle size with respect to temperature. At low temperature the p(NIPAM-*co*-DABP-*co*-AAc) particles display a swollen transition and a higher particle diameter. In contrast, the swollen particles expel water from inside and exhibit a shrunken state at higher temperature, and thus there is a reduction of the particle size. The obtained data were fit to a Boltzmann sigmoidal curve fitting function using the Origin Lab program software and the LCST was determined. From the data, the LCST of the synthesized p(NIPAM-*co*-DABP-*co*-AAc) was found to be around 30 °C. The obtained findings are also in good agreement with the results obtained from DSC analysis. Besides, we observed a significant decrease in the particle size when the temperature was more than 30 °C. This observation is attributed to the change in the conformation of the polymeric chain. The polymers change their conformation from loose coils to a condensed dehydrated state at or above the LCST. The above-revealed characteristics of pNIPAM permits the release of preloaded drug molecules from the p(NIPAM-*co*-DABP-*co*-AAc) matrix in response to the physiological temperature (>30 °C) and provide a new way to formulate temperature-triggered drug delivery systems.[24,25,34]

Furthermore, the pH-responsive behavior of the synthesized system was also investigated using the DLS technique, and a change in the particle size as a result of pH changes of solution was recorded (Fig. 8). We hypothesized that an increase in the particle size is observed when the pH is more than the pK_a value of AAc due to acid ionization, with a further decrease in the diameter when the pH is less than the pK_a of AAc due to the
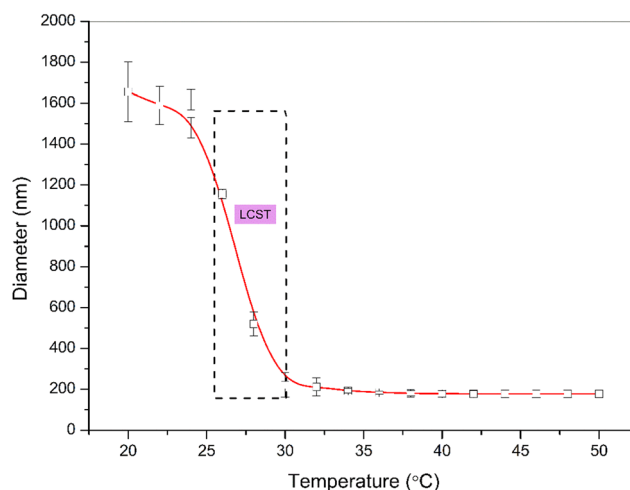

Fig. 6 Deconvoluted MALDI-ToF spectrum of p(NIPAM-*co*-DABP-*co*-AAc).

Fig. 7 Temperature dependent hydrodynamic diameter of the p(NIPAM-*co*-DABP-*co*-AAc) hydrogel to determine the LCST of the system.

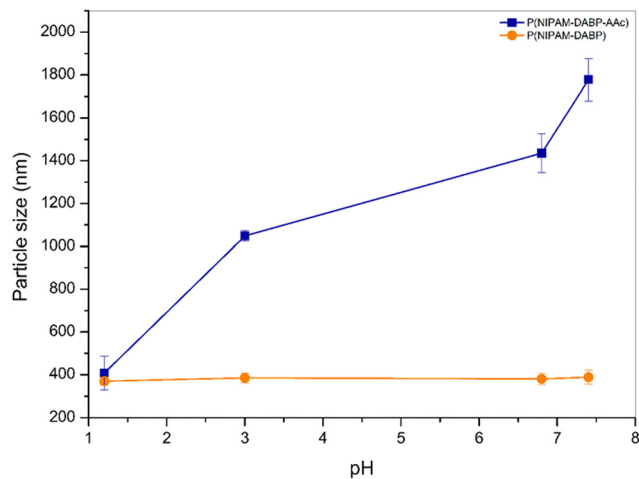This journal is © The Royal Society of Chemistry 2024

J. Mater. Chem. B, 2024, **12**, 5098–5110 | **5105**

Fig. 8 pH responsive hydrodynamic diameter of the p(NIPAM-*co*-DABP-*co*-AAc) hydrogel.

Fig. 9 ^{1}H NMR spectrum of p(NIPAM-*co*-DABP-*co*-AAc) in D_2O at 25 and 50 °C.

acid neutralization. This is due to the fact that at basic pH (pH > pK_a) the synthesized hydrogel system is negatively charged and shows a swollen configuration due to the coulombic repulsion between charges, resulting in the generation of osmotic pressure in the hydrogel system.[25] From Fig. 8, on the other hand, no pH-responsive behavior was observed for the p(NIPAM-*co*-DABP) system; however, the system composed of AAc, *i.e.*, p(NIPAM-*co*-DABP-*co*-AAc) demonstrates a desirable pH response. We observed an increase in the diameter as the pH of the solution increased, and the drastic increase in the diameter was observed when the pH was more than the pK_a of AAc (pH > pK_a: 6 > 4.25).

As PNIPAM is a well-known temperature-sensitive polymer, we hypothesized that the copolymer composed of PNIPAM and AAc should retain their thermosensitivity. Fig. S13 (ESI†) shows the temperature-responsive behavior of the synthesized copolymer p(NIPAM-*co*-DABP-*co*-AAc) at the indicated solution pH. We observed a decrease in the particle size when the temperature of the pH solution increased from 20 °C to 50 °C at pH 1.2 and 7.4.

To elucidate the molecular level temperature-responsive behaviour of the synthesized P(NIPAM-*co*-DABP-*co*-AAc) triblock copolymer, we performed variable temperature ^{1}H NMR spectroscopy using D_2O as a solvent at two different temperatures *i.e.*, 25 °C and 50 °C. The obtained spectra are shown in Fig. 9. The more resonant proton peaks, which are attributed to the DABP and PNIPAM chains, are selected to determine the chemical shifting of protons with respect to the temperature. The temperature-responsive polymers show reversible coil-to-globule transition at or above the LCST, which leads to the stronger ^{1}H coupling due to decrease in the segmental mobility of hydrophobic groups.[35] It is well known that the coil-to-globule transition of the PNIPAM moiety occurs above the LCST, which is associated with the dehydration of the polymer chain,[36] due to the loss of water molecules from the hydrophobic group in the PNIPAM based copolymer chain. Hence, the proton shift of these segments is observed in downfield
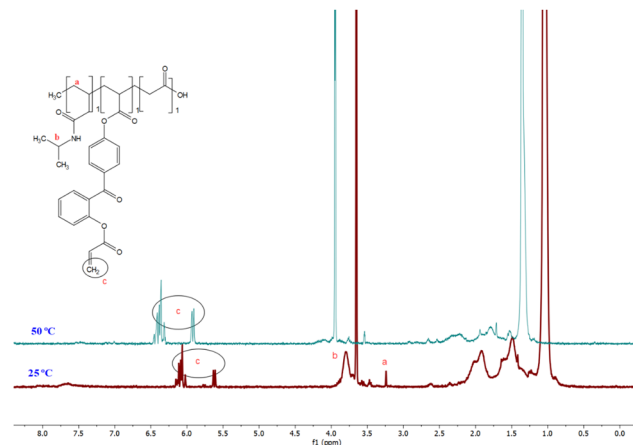
along with decrease in the intensity with respect to the increasing temperature.[36,37] Hence, holding this hypothesis, the ^{1}H NMR spectrum of the synthesized triblock copolymer was recorded at 25 °C (below LCST) and 50 °C (above LCST). The dominant peaks 'a', 'b', and 'c', which are specifically related to the hydrophobic segments in the p(NIPAM-*co*-DABP-*co*-AAc) triblock copolymer, are considered for further evaluation (Fig. 9). Interestingly the obtained spectra reveal the peak shift of the hydrophobic DABP proton 'c' towards downfield in the case of the NMR spectra obtained at 50 °C compared to the NMR spectra taken at 25 °C. On the other hand, the peak signals corresponding to the NIPAM segment (peaks a and b) are hardly detectable after the phase transition at 50 °C. From the obtained results, we can conclude that the obtained findings are in good agreement with the designed hypothesis and previously available literature reports,[35,36,38] and the findings further confirm the dehydration of hydrophobic segments in the p(NIPAM-*co*-DABP-*co*-AAc) triblock copolymer at or above the LCST, subsequently proving the thermosensitivity of the p(NIPAM-*co*-DABP-*co*-AAc) triblock copolymer.

Finally, the conventional FT-IR and UV-visible spectroscopy was performed to determine the pH responsive behaviour of the synthesized copolymer. The obtained spectra are shown in Fig. S14 (ESI†). The analysis of the obtained results was performed based on the hypothesis that at pH > pK_a of AAc, p(NIPAM-*co*-DABP-*co*-AAc) is in deprotonated form, *i.e.*, CO_2^- form will dominate, and when the pH of the solution is less than the pK_a of AAc, the copolymer will exist as free carboxylic acid, *i.e.*, COOH without any charge. Fig. S14a (ESI†) shows the FT-IR spectra of p(NIPAM-*co*-DABP-*co*-AAc) at four different pH values. The canine teeth-shaped peaks around 1070 and 985 cm^{-1} were observed in the case of the FT-IR spectrum of p(NIPAM-*co*-DABP-*co*-AAc) at pH 6.8 and 7.4. These peaks correspond to the asymmetric and symmetric stretching of the $-CO_2^-$ group.[39] In the case of pH 1.2 and 3.0, the absence of the $-CO_2^-$ group peaks in the FT-IR spectrum indicates a fully protonated form of the copolymer at acidic pH. Hence, the obtained data confirm the conversion of protonated to deprotonated form of the copolymer as the pH of the solution

5106 | *J. Mater. Chem. B*, 2024, **12**, 5098–5110

This journal is © The Royal Society of Chemistry 2024

increases, indicating that the prepared copolymer can swell and collapse as the pH is increased/decreased. Furthermore, the same phenomenon was observed in the case of UV-visible spectroscopy studies. The absorbance above 300 nm was observed when the pH of the solution was more than the pK_a of AAc, which is attributed to the carboxylate ions[40] (Fig. S14b, ESI†). The obtained results convey pH induced deprotonation and protonation of the synthesized copolymer at basic and acidic pH respectively.

3.5. Cytotoxicity assessment

In order to study the biomedical applicability of the synthesized copolymer, an *in vitro* cytocompatibility experiment was performed. MTT assay is a well-established, preliminary, and easy method to determine the biocompatibility of such copolymers before proceeding to the *in vivo* applications. The cytotoxicity against HEK-239 and HT-29 was determined as a function of copolymer concentration. The obtained data are shown in Fig. 10, indicating more than 90% cell viability at the highest copolymer concentration of 1000 μg mL^{-1}, which is considered as a good cytocompatibility for biomedical applications. Hence, MTT assay reveals that the synthesized p(NIPAM-*co*-DABP-*co*-AAc) triblock copolymer exhibited no obvious cytotoxicity. Furthermore, detailed *in vivo* toxicity studies must be carried out to prove the synthesized copolymer as a '*biomaterial*' for various biomedical and drug delivery applications.

3.6. Acute oral toxicity study

3.6.1. General appearance. All experimental rats were crucially observed for any signs of toxicity such as weight loss, general behaviour, mortality, *etc.* as per the OECD-423 guidelines. The obtained data are shown in Table S1 (ESI†). All the animals showed no signs of toxicity with normal general appearance observations. Furthermore, the increase in the body weight is considered as an initial sign of various organ toxicity and metabolic dysfunction. The body weight of each rat was recorded before and after oral dosing of the synthesized compound and compared with the control group. The obtained data are shown in Table S1 (ESI†), indicating no significant change in the body weights of all treated rats up to the 14th day.
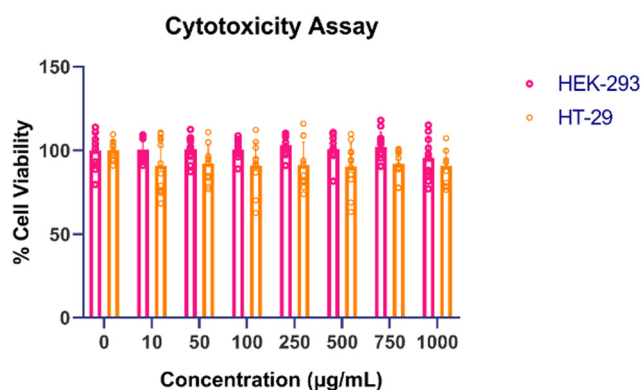

Fig. 10 % Cell viability as a function of p(NIPAM-*co*-DABP-*co*-AAc) concentration.

Overall, the findings convey the initial safety of the synthesized compound after oral administration.

3.6.2. Hematological and biochemical analyses. The haematological parameters and biochemical parameters were determined before and after dosing and compared with the control group; the obtained data are shown in Table S2 and Fig. S15 (ESI†). The obtained data convey that all the haematological and biochemical parameters for control and test groups were found to be within the normal physiological range[41,42] and did not display any significant difference when compared with the control group.

3.6.3. Histopathology. To observe the organ-level toxicological impact of the synthesized copolymer, the microscopic histopathological characterization of the liver, kidneys (the major organs involved in metabolism), and small intestine (the major organ responsible for absorption) was performed, and the data are shown in Fig. 11. The microscopic histopathological evaluation of liver sections of SD rats from the control and treated groups was performed using 10× and 20× magnifications. Normal lobular architecture and portal tract were observed in the control group. The liver section after the treatment with 2000 mg kg^{-1} copolymer displayed normal lobular architecture, central veins, and sinusoids. There was not any kind of the toxic signs like inflammatory patches, fatty changes, and fibrosis in hepatocytes. The kidney histological sections of both control and copolymer treated SD rats were examined using 10× and 20× magnifications. The cortex, medulla, and glomeruli structure from the sections of both groups were found to be normal and intact. The sections demonstrated normal interstitial conditions and no inflammation or necrosis was present. Finally, histopathological evaluation of the intestinal section showed the normal crypt, mucosal lining, and villi upon examining under 10× and 20× magnifications. Structures present in the intestine are intact and normal. There are no inflammation and necrosis observed in the intestinal cell lining after 14 days of experimental period. Overall, no evidence of pathological damage or toxicity of the synthesized copolymer was observed, indicating it as a potential '*biomaterial*'.

3.7. Dual-stimuli responsive/triggered drug release

Various studies have shown the effectiveness of the multiple drug treatment to cure various diseases[43,44] and also simultaneous delivery of two or more drugs to minimize the adverse reactions of certain drugs and minimize the drug resistance.[45] Here, we developed a new material, which has the ability to control or trigger the release of a small molecule(s) in response to physiological conditions, which will improve the effectiveness of the individual therapy. In this respect, thanks to the NIPAM for its tunable properties, the design of a triblock copolymer comprises hydrophilic and hydrophobic units, which will improve the drug loading capacity and drug release with respect to the LCST of the system, and addition of AAc adds a new dimension to the material, making it a temperature and pH dual responsive system, which could effectively control the drug release in response to the external stimuli with myriad applications of this material in biomedical and pharmaceutical fields. Here we showed the ability
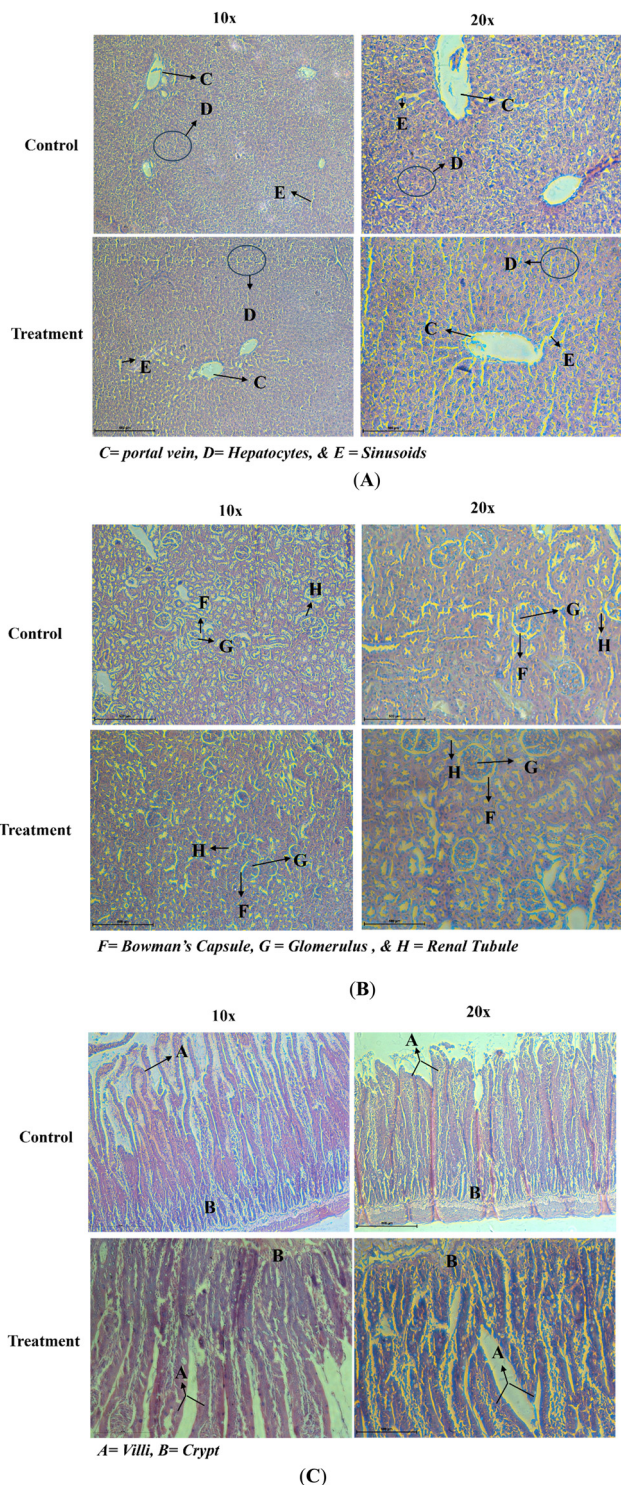
This journal is © The Royal Society of Chemistry 2024

J. Mater. Chem. B, 2024, **12**, 5098–5110 | **5107**

C= portal vein, D= Hepatocytes, & E = Sinusoids

(A)

F= Bowman's Capsule, G = Glomerulus , & H = Renal Tubule

(B)

A= Villi, B= Crypt

(C)

Fig. 11 Histopathological sections of (A) liver, (B) kidneys, and (C) small intestine (H and E staining, magnification 10× and 20×).

of the synthesized triblock copolymer p(NIPAM-*co*-DABP-*co*-AAc) to release entrapped 5-FU in a controlled and triggered fashion in response to temperature and pH.

3.7.1. 5-FU release observations by changing temperature. The temperature-dependent release of 5-FU is shown in Fig. 12(A). To investigate the temperature-dependent release of 5-FU, the

release was performed at two different temperatures at 24 °C and 40 °C in an aqueous medium. The obtained findings reveal that the release rate of 5-FU is more at lower temperature and slower at higher temperature. This observation was attributed to the temperature-dependent shrinkage of the p(NIPAM-*co*-DABP-*co*-AAc)-based hydrogel. As a result at temperatures higher than LCST, the collapsed pores of the hydrogel matrix restrict the diffusion pathway of 5-FU from the hydrogel matrix to the solution leading to the slower release of 5-FU. These results revealed that the prepared PNIPAM based hydrogel matrix showed a great impact on the controlled 5-FU release with respect to the change in temperature. The obtained findings also align with the available literature reports.[8,46] Furthermore, p(NIPAM-*co*-DABP-*co*-AAc) showed a minimal release of 5-FU at elevated temperature, which is near the body temperature, suggesting its ability to sustain and fasten the release of 5-FU at higher and room temperatures, respectively.

3.7.2. 5-FU release observations by changing pH. Next, we investigate the ability of p(NIPAM-*co*-DABP-*co*-AAc) to control the release of 5-FU *via* another external factor to which the synthesized hydrogel responds, *i.e.*, pH. For this study, the entrapment of 5-FU was achieved using a swelling diffusion method at body temperature, showing a maximum entrapment efficiency of around 90%. The *in vitro* release study of 5-FU from the prepared matrix was performed by varying the pH of the solution from 1.2 to 6.8 at constant temperature (Fig. 12(B)). As confirmed by the DLS, UV, and FT-IR spectroscopy techniques, p(NIPAM-*co*-DABP-*co*-AAc) showed a pH-responsive behaviour and is able to release the entrapped 5-FU when the pH of the medium is more than the pK_a. As shown in Fig. 12(B), around 17% of cumulative 5-FU release was observed at pH 1.2 and it is almost constant for up to 4.0 h (Fig. 12(B) zoom in). This is due to the fact that at pH $<$ pK_a, the synthesized hydrogels were in the collapsed state at a temperature higher than the LCST ($>$30 °C), which blocks the 5-FU diffusion pathway. After 4.0 h, the pH of the medium was adjusted to 6.8, and the 5-FU release pattern was observed. Initially, no marked release was observed, and this might be due to the time taken by the hydrogel to respond to the environmental pH change. Overall, around 80% of release was observed at pH 6.8 within 24 hours. At basic pH, the deprotonated form of hydrogels absorbs more release medium and showed drastic swelling behaviour, leading to the faster release of 5-FU. The same kind of behaviour was also observed in the SEM study. As shown in Fig. S16a and b (ESI†), the drastic decrease in the particle size was observed when the pH of the solution was less than the pK_a of AAc (Fig. S16a, ESI†). In contrast, at basic pH, we observed significant swelling with visualization of pores on the hydrogel surface, which further supports the rapid release of 5-FU in basic media (Fig. S16b, ESI†). Therefore, the LCST and swelling behaviour of the designed hydrogel can be naturally mediated by the pH difference in the gastro-intestinal tract, which may be an attractive tool for smart oral drug delivery systems.

4. Conclusion

In summary, a dual stimuli-responsive hydrogel, named p(NIPAM-*co*-DABP-*co*-AAc), was prepared using DABP as a
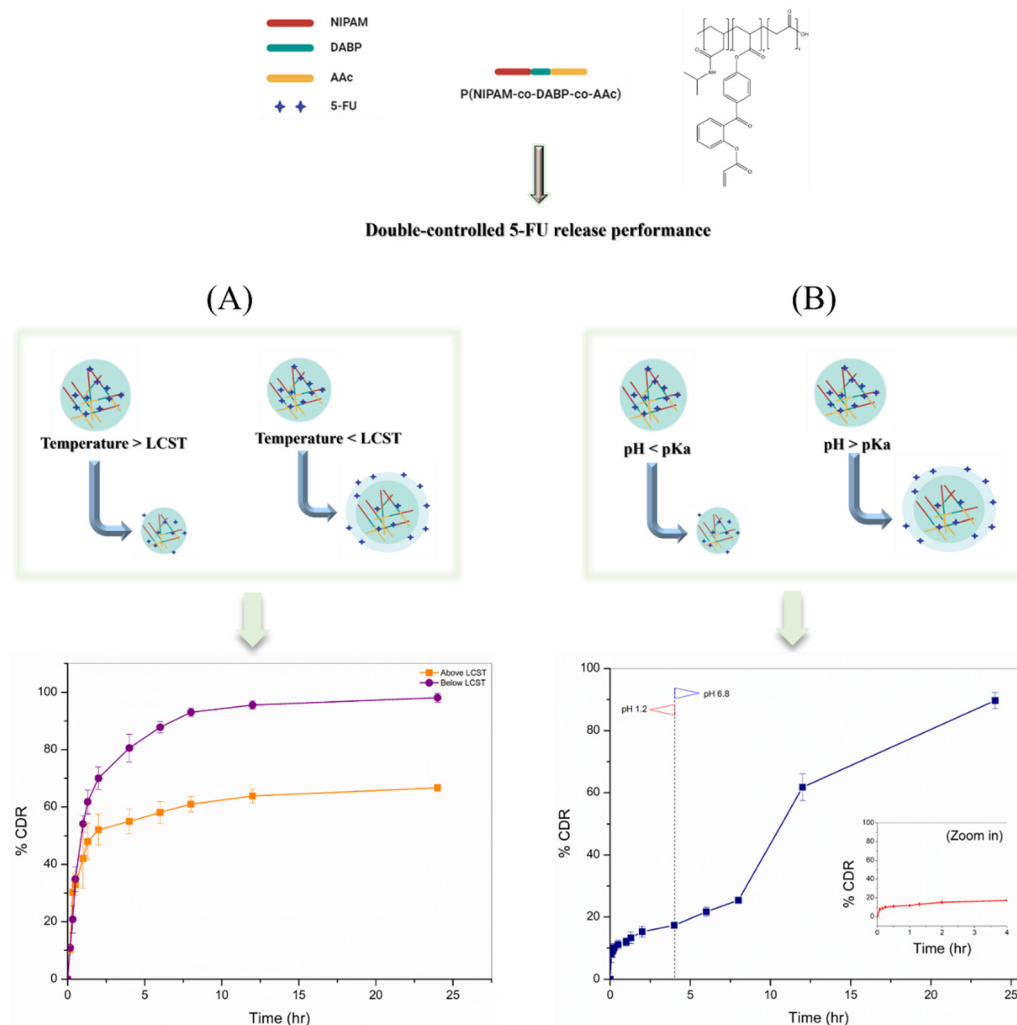
5108 | *J. Mater. Chem. B*, 2024, **12**, 5098–5110

This journal is © The Royal Society of Chemistry 2024

Fig. 12 *In vitro* release of 5-FU from the p(NIPAM-*co*-DABP-*co*-AAc) hydrogel: (A) temperature responsive release behaviour and (B) pH responsive release behaviour.

crosslinker by free radical copolymerization. The used two approaches such as step wise synthesis and one pot synthesis enabled the hydrophobic crosslinker to successfully react with PNIPAM and AAc to form a new dual temperature and pH-responsive copolymer and hydrogel. The developed hydrogel was thoroughly characterized for its chemical and physical properties using various analytical tools such as NMR, XPS, FT-IR, DSC, TGA, XRD, DLS, *etc.* We demonstrated that the controlled concentration of DABP and AAc generates a hydrogel with LCST around body temperature and is able to respond to the physiological pH change. In this respect, the LCST of the synthesized copolymer and hydrogel was found to be around 30 °C by the DLS technique. The synthesized hydrogel exhibits thermo and pH-sensitive swelling/deswelling behaviour that can be facilitated by environmental temperature and pH changes, leading to different 5-FU release observations under different temperature and pH conditions. The MTT assay reveals more than 90% of cell viability at higher dose and *in vivo* acute oral toxicity findings confirm the excellent biocompatibility of synthesized p(NIPAM-*co*-DABP-*co*-AAc). The

in vitro 5-FU release study revealed that the release of 5-FU is sustained at higher temperature, showing around 50% of 5-FU release in 24 h, in contrast to that at lower temperature where an almost 90% release was observed in 24 h. In addition to this, the same hydrogel system was able to suppress the 5-FU release in an acidic environment, maintaining a considerable plateau state, while it was significantly enhanced as soon as the pH of the medium was changed to basic conditions. The overall findings demonstrate the significant use of such copolymers for the tunable release of single or multiple drugs from a single copolymer matrix. In the future, we will further integrate the synthesized hydrogel system with 3D printing technology for the fabrication of personalized and effective drug delivery devices for gastrointestinal/colorectal cancer with detailed *in vivo* animal studies. Altogether, the findings provide an experimental approach to generate new copolymers that can release the drug molecules when desired. Furthermore, the synthesized thermal and pH-triggered hydrogel could open a new era in the field of self-regulated drug delivery in response to the physiological changes.

Conflicts of interest

There are no conflicts to declare.

Acknowledgements

References

1 T. R. Hoare and D. S. Kohane, *Polymer*, 2008, **49**, 1993–2007.
2 S. Bucatariu, G. Fundueanu, I. Prisacaru, M. Balan, I. Stoica, V. Harabagiu and M. Constantin, *J. Polym. Res.*, 2014, **21**, 1–12.
3 L. Klouda, *Eur. J. Pharm. Biopharm.*, 2015, **97**, 338–349.
4 T. T. Koev, H. C. Harris, S. Kiamehr, Y. Z. Khimyak and F. J. Warren, *Carbohydr. Polym.*, 2022, **289**, 119413.
5 D. Kang, Z. Liu, C. Qian, J. Huang, Y. Zhou, X. Mao, Q. Qu, B. Liu, J. Wang and Z. Hu, *Acta Biomater.*, 2023, **165**, 19–30.
6 M. O. Teixeira, E. Marinho, C. Silva, J. C. Antunes and H. P. Felgueiras, *J. Drug Delivery Sci. Technol.*, 2023, **89**, 105066.
7 N. B. Allen, B. Abar, L. Johnson, J. Burbano, R. M. Danilkowicz and S. B. Adams, *Bioprinting*, 2022, **26**, e00196.
8 S. Guo, D. Wong, S. Wang, R. Gill and M. J. Serpe, *J. Mater. Chem. B*, 2022, **10**, 4416–4430.
9 R. Keidel, A. Ghavami, D. M. Lugo, G. Lotze, O. Virtanen, P. Beumers, J. S. Pedersen, A. Bardow, R. G. Winkler and W. Richtering, *Sci. Adv.*, 2018, **4**, eaao7086.
10 S. K. Wypysek, A. Scotti, M. O. Alziyadi, I. I. Potemkin, A. R. Denton and W. Richtering, *Macromol. Rapid Commun.*, 2020, **41**, 1900422.
11 B. Garcia-Pinel, A. Ortega-Rodríguez, C. Porras-Alcalá, L. Cabeza, R. Contreras-Cáceres, R. Ortiz, A. Díaz, A. Moscoso, F. Sarabia and J. Prados, *Artif. Cells, Nanomed., Biotechnol.*, 2020, **48**, 1022–1035.
12 N. Murthy, M. Xu, S. Schuck, J. Kunisawa, N. Shastri and J. M. Fréchet, *Proc. Natl. Acad. Sci. U. S. A.*, 2003, **100**, 4995–5000.
13 I. Sanzari, E. Buratti, R. Huang, C. G. Tusan, F. Dinelli, N. D. Evans, T. Prodromakis and M. Bertoldo, *Sci. Rep.*, 2020, **10**, 6126.
14 R. Elancheliyan, G. Del Monte, E. Chauveau, S. Sennato, E. Zaccarelli and D. Truzzolillo, *Macromolecules*, 2022, **55**, 7526–7539.
15 A. A. Karanastasis, G. S. Kenath, D. Andersen, D. Fokas, C. Y. Ryu and C. K. Ullal, *J. Colloid Interface Sci.*, 2020, **568**, 264–272.
16 J. C. Breger, C. Yoon, R. Xiao, H. R. Kwag, M. O. Wang, J. P. Fisher, T. D. Nguyen and D. H. Gracias, *ACS Appl. Mater. Interfaces*, 2015, **7**, 3398–3405.
17 Q. Huang, L. Wang, H. Yu and K. Ur-Rahman, *J. Controlled Release*, 2019, **305**, 50–64.
18 K. Muraleedharan, *Int. J. Greenhouse Gas Control*, 2017, **58**, 62–70.
19 S. Tang, M. Floy, R. Bhandari, M. Sunkara and A. J. Morris, *Synthesis*, 2017, 7–2017.
20 Y. H. Bae, T. Okano and S. W. Kim, *Pharm. Res.*, 1991, **8**, 531–537.
21 S. J. Lue, C.-H. Chen and C.-M. Shih, *J. Macromol. Sci., Part B*, 2011, **50**, 563–579.
22 H. Bera, Y. F. Abbasi, V. Gajbhiye, K. F. Liew, P. Kumar, P. Tambe, A. Azad, D. Cun and M. Yang, *Mater. Sci. Eng., C*, 2020, **110**, 110628.
23 G. Stoychev, N. Puretskiy and L. Ionov, *Soft Matter*, 2011, **7**, 3277–3279.
24 P. Suryavanshi, S. Kawre, M. Maniruzzaman, K. Seth and S. Banerjee, *Chem. Pap.*, 2023, **77**, 1–10.
25 A. Ahiabu and M. J. Serpe, *ACS Omega*, 2017, **2**, 1769–1777.
26 OECD, *Test No. 423: Acute Oral toxicity - Acute Toxic Class Method*, 2002.
27 X. Gao, Y. Cao, X. Song, Z. Zhang, C. Xiao, C. He and X. Chen, *J. Mater. Chem. B*, 2013, **1**, 5578–5587.
28 D. L. Pavia, G. M. Lampman, G. S. Kriz and J. Vyvyan, *Introduction Spectrosc.*, 2001, 14–106.
29 M. Santhamoorthy, T. T. Vy Phan, V. Ramkumar, C. J. Raorane, K. Thirupathi and S.-C. Kim, *Polymers*, 2022, **14**, 4128.
30 S. Tang, M. Floy, R. Bhandari, M. Sunkara, A. J. Morris, T. D. Dziubla and J. Z. Hilt, *ACS Omega*, 2017, **2**, 8723–8729.
31 Y.-T. Shieh, P.-Y. Lin and S.-W. Kuo, *Polymer*, 2018, **143**, 258–270.
32 C.-C. Diao and C.-C. Wu, *ACS Omega*, 2022, **7**, 8697–8705.
33 Z. Wang, Q. Zhang, H. Shen, P. Yang and X. Zhou, *Front. Chem.*, 2021, **9**, 698297.
34 J. Bocanegra-Flores, C. Haro-Pérez, D. Reyes-Contreras and L. Rojas-Ochoa, *Front. Phys.*, 2022, 824.
35 Y. Zhou and P. Wu, *Polymer*, 2018, **153**, 250–261.
36 L. Tavagnacco, E. Zaccarelli and E. Chiessi, *Phys. Chem. Chem. Phys.*, 2018, **20**, 9997–10010.
37 H. Wolf, E. Nadine, K. Anne-Larissa, D. Patrick and W. Ralf, 2015.
38 S. Sun, P. Wu, W. Zhang, W. Zhang and X. Zhu, *Soft Matter*, 2013, **9**, 1807–1816.
39 B. C. Smith, *Spectroscopy*, 2018, **33**, 20-23–20-23.
40 L. Wang, C. Zhang, H. Mestankova, F. Wu, N. Deng, G. Pan, M. Bolte and G. Mailhot, *Photochem. Photobiol. Sci.*, 2009, **8**, 1059–1065.
41 W. A. Q. (Loeb, FW.), *The Clinical Chemistry of Laboratory Animals*, Taylor & Francis, USA, Philadelphia, 2nd edn, 1999.
42 Q. He, G. Su, K. Liu, F. Zhang, Y. Jiang, J. Gao, L. Liu, Z. Jiang, M. Jin and H. Xie, *PLoS One*, 2017, **12**, e0189837.
43 Y. Liu, Y. Ran, Y. Ge, F. Raza, S. Li, H. Zafar, Y. Wu, A. C. Paiva-Santos, C. Yu and M. Sun, *Pharmaceutics*, 2022, **14**, 652.
44 Y.-W. Yeh, C.-C. Huang, W.-S. Kuo, T.-L. Liao, T.-L. Tsai and P.-C. Wu, *ACS Omega*, 2023, **8**, 10278–10287.
45 W. Wang, Y. Xiong, X. Hu, F. Lu, T. Qin, L. Zhang, E. Guo, B. Yang, Y. Fu and D. Hu, *Acta Biomater.*, 2023, **157**, 428–441.
46 Y. K. Kim, E.-J. Kim, J. H. Lim, H. K. Cho, W. J. Hong, H. H. Jeon and B. G. Chung, *Nanoscale Res. Lett.*, 2019, **14**, 1–9.

5110 | *J. Mater. Chem. B*, 2024, **12**, 5098–5110

This journal is © The Royal Society of Chemistry 2024